INSTITUTE OF PHYSICS PUBLISHING JOURNAL OF MICROMECHANICS AND MICROENGINEERING

J. Micromech. Microeng. **16** (2006) S248–S253 doi:10.1088/0960-1317/16/9/S12

Increasing μDMFC efficiency by passive CO_2 bubble removal and discontinuous operation

C Litterst[1], S Eccarius[2], C Hebling[2], R Zengerle[1] and P Koltay[1]

[1] Laboratory for MEMS Applications, University of Freiburg—IMTEK, Georges-Koehler-Allee 106, D-79110 Freiburg, Germany
[2] Fraunhofer Institute for Solar Energy Systems, Heidenhofstr 2, D-79110 Freiburg, Germany

E-mail: litterst@imtek.de

Received 30 January 2006, in final form 31 January 2006
Published 11 August 2006
Online at stacks.iop.org/JMM/16/S248

Abstract

A new concept that enables fully passive CO_2 gas bubble removal in micro direct methanol fuel cells (μDMFCs) is presented. The original concept behind the presented degassing structure (flowfield) is based on microchannels with a T-shaped cross section. These channels have defined tapering angles over their cross section (α) and along their axis (β). The tapered channel design creates an intrinsic transport mechanism that removes the gas bubbles from the electrodes by capillary forces only. Computational fluid dynamic (CFD) simulations have been used to determine applicable opening angles of $\alpha = 5^\circ$ and $\beta = 1.5^\circ$. The experimental verification was done by using a transparent flowfield to show the passive bubble removal as well as with a fully operational μDMFC. During the operation, the fuel cell delivered an output of up to 8 mW cm^{-2} without the need for external pumping in short-term measurements. During the long-term measurements, discontinuous pumping showed the highest fuel cell efficiency compared to the continuously pumped fuel supply.

1. Introduction

Assisting or even replacing secondary batteries by fuel cells has been a research goal throughout the recent years [1, 2]. The most promising type of fuel cell for applications with low power consumption is the μDMFC since methanol allows instant refuelling and furthermore safe fuel storage as opposed to hydrogen. In order to achieve real competitive fuel cell systems compared to the battery market several problems still have to be solved.

One of these problems is caused by the production of carbon dioxide (CO_2) during the oxidation of methanol on the anode side of the fuel cell. This reaction results in a two-phase flow of the liquid fuel and the gaseous CO_2. The gas bubbles reduce the fuel cell's efficiency since they block parts of the membrane electrode assembly (MEA), become immobile or even block a channel completely, a problem that is well known in microfluidics [3, 4]. Another problem is the continuous supply of methanol to the anode compartment. Typically, this methanol supply is realized by a continuous flow forced by micropumps that consume a part of the energy produced by the fuel cell. The convective flow is also used to flush out dissolved CO_2 before bubbles can block the channels and the MEA. However, one has to keep in mind that micropumps typically have a low efficiency [5] and thus consume a non-negligible amount of energy. Due to this, it is favourable to reduce the pumping effort or even to completely abandon a pump in a μDMFC system. This is only possible if the gas bubbles are removed passively from the liquid methanol. In this paper, a flowfield layout is presented that removes the gas bubbles by capillary forces only and thus also improves the fuel cell system's efficiency since continuous convective flow is not required for operation.

2. Flowfield concept

In small dimensions surface forces cannot be neglected and often cause severe problems that can only be overcome with considerable effort. Nevertheless, such forces can also be

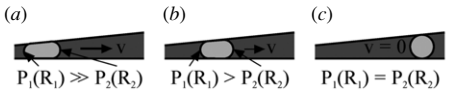

Figure 1. (*a*) and (*b*) Two-dimensional draft of gas bubble movement in a tapered channel, driven by different capillary pressures. (*c*) Equilibrium state with no bubble movement.

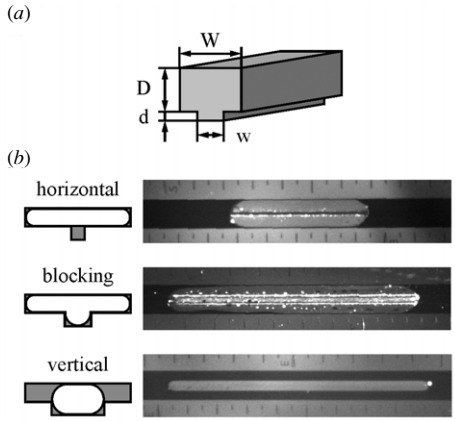

Figure 2. (*a*) Sketch of the original T-shaped channel design [4]. (*b*) Photographs of the three possible gas bubble positions in a liquid (dark grey) filled T-shaped channel [6].

of advantage in certain applications. Special microchannel designs, for example, have been reported to increase the mobility of gas bubbles trapped in liquid-filled channels [4, 6]. The channel geometry and the capillary forces can be used to shape bubbles and increase their mobility. A further improvement of the microchannel design presented in [4, 6] allows passive CO_2 gas bubble removal from the anode flowfield of a μDMFC as described in the following.

2.1. Working principle

In brief the working principle of the flowfield layout is based on the non-uniform capillary pressure $\left(P_{\text{cap}} = \sigma\left(R_x^{-1} + R_y^{-1}\right)\right)$ exerted by a tapered channel. The considered situation is sketched in figure 1. The two distant ends of an elongated gas bubble exhibit different curvatures R and thus experience different capillary pressures P. The pressure difference forces the bubble to move towards the wider channel part until both capillary pressures are in equilibrium as sketched in figure 1(*c*). In this case, the bubble takes on a spherical shape and the movement stops. In the fuel cell application, the bubble might even increase in size during its movement along the channel. This might happen, if one wall is formed by the MEA and other bubbles growing there are wiped off and merged with the passing bubble.

2.2. General layout

A prerequisite for a sufficiently fast bubble movement is a channel design, allowing liquid to bypass the gas bubble. A design that provides such a bypass is a channel with a T-shaped cross section as shown in figure 2(*a*). This channel design has already been presented in [4] together with an analytical model describing the rise of a gas bubble in this specific geometry.

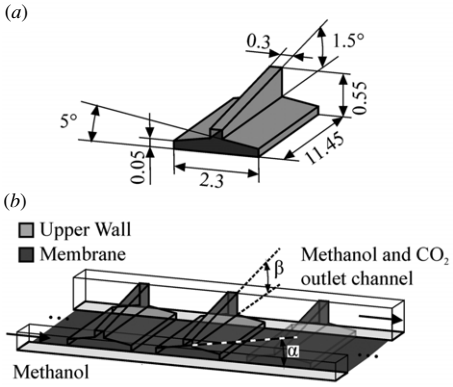

Figure 3. (*a*) Sketch of the channel dimensions of the test samples in millimetres (not to scale). (*b*) Draft of one side of the flowfield indicating the supply and the outlet channel as well as the T-shaped parallel channels with their tapering angles α and β.

Based on this work and the study of geometric variations of the T-shaped cross section, Litterst *et al* presented a model to determine the bubble position in channels with this cross-sectional layout [6]. Depending on the geometry parameters (W, w, D, d) shown in figure 2(*a*), any one of the three stable bubble positions referred to as 'horizontal', 'blocking' and 'vertical' can be adopted as shown in figure 2(*b*).

Since the T-shaped cross section itself does only influence the bubble position inside the channel but does not provide the necessary capillary forces to move the gas bubble passively, tapered channel walls have been added to the basic T-shaped channel layout as shown in figure 3(*a*). However, the channel dimensions have been chosen to guarantee a vertical bubble position by assuming the worst case at the shallowest part of the central channel. To form a flowfield for the fuel cell, the T-shaped tapered channels are arranged as two parallel rows connected to a central supply channel. The other side of the channel is connected to an outlet channel placed on the outer side of the flowfield. In each of the two rows, 18 T-shaped channels are placed with a spacing of 0.3 mm between each other as indicated in figure 3(*b*). The T-shaped channels are tapered in two dimensions: first symmetrically by a tapering angle $\alpha = 5^\circ$ across their profile and by an angle $\beta = 1.5^\circ$ along their longitudinal section opening towards the outlet channel.

As shown in figure 3(*b*), the catalyst-coated membrane or a gas diffusion layer (e.g. carbon paper or a metal mesh) forms the bottom side of the parallel channels while the remaining channel walls are formed by the substrate. Since the MEA covers the whole bottom of the T-channels, the largest possible area is used for fuel cell operation. The bubbles can grow on that surface and as soon as a bubble comes into contact with the upper wall, capillary action starts to move it towards the larger cross section of the channel. Due to the ongoing reaction, the bubble size still increases and thus the bubble is forced to deform its spherical shape into a stretched oval shape as already sketched in figure 1. The pressure gradient, evoked by the unbalanced capillary forces, yields a bubble movement towards the central part of the T-shaped channel. This motion continues towards the central channel as already described above for tapered channels. Once the central part is reached, the bubble takes on a shape that only fills the central part due to the T-shaped design. This behaviour has basically been

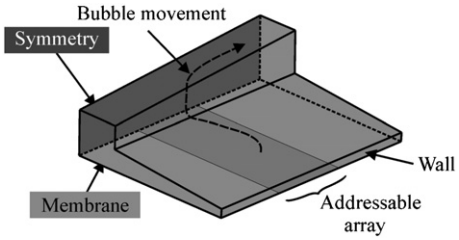

Figure 4. Simulation model and the applied boundary conditions as well as the expected direction of bubble movement.

avowed by the authors in [6]. Once the bubble is inside the middle channel the tapering again makes the bubble move to the final outlet.

3. Simulation

Prior to the manufacture of test samples the basic working principle has been proved by CFD simulations with the use of the software package CFD-ACE+ (ESI CFD, Inc., Huntsville, AL) version 2004.0.25. After some preliminary tests with one defined bubble in a tapered channel and its movement therein, the target of the simulations switched towards modelling an ensemble of bubbles in the flowfield. To reduce the simulation time as much as possible only a small representative part of one of the tapered channels has been modelled. The model has a length of 600 μm compared to 11.45 mm of the whole tapered channel and furthermore it is simplified by using a symmetry boundary condition in the centre of the cross section (cf figure 4). The ends of the channel are modelled as outlet while the remaining boundaries are treated as walls from the substrate or MEA, both with a contact angle of $\theta = 0^\circ$. The surface that represents the MEA is divided into three parts, where the outer parts have a fixed wall boundary condition and the central part consists of an addressable array of 20×50 quadratic surfaces that also have a predefined wall boundary condition. The two outer parts of the MEA have been implemented to avoid unphysical effects due to gas bubbles coming into contact with one of the outlets. Such a contact causes the bubble to be sucked through the boundary condition. Due to the high number of surfaces, the total number of cells yields 150 000 with a minimum cell size of 70.1 μm^3. Thereby the largest aspect ratio was 1.8. In all dimensions the grid points had been almost evenly distributed with 101 grid points along the channel, 121 over the channel width and 24 over the channel depth.

Since in the experiments the CO_2 bubbles can develop randomly all over the MEA surface, a method has been developed to mimic this behaviour of bubble development in the simulation. For this reason, the addressable array has been introduced. Prior to each simulation run with a duration of 0.5 ms a script is applied to the model that automatically sets the boundary conditions in the addressable array. Within the script a routine randomly selects 10 of the 1000 surfaces of the array and changes the boundary condition to a gas inlet with a defined mass flow rate. The mass flow rate of CO_2 through each inlet is based on the estimation that a typical current density of 100 mA cm^{-2} generates 0.26 ml min^{-1} cm^{-2} of CO_2. After 0.5 ms, the simulation stops and the script

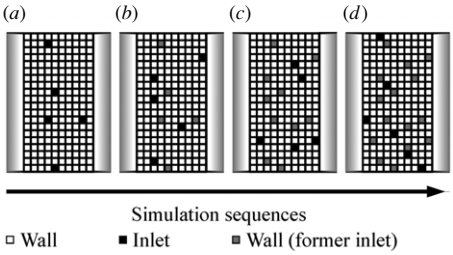

Figure 5. Example sequence of the switching inlet boundary conditions in the addressable array of the MEA. In each simulation five surfaces are set as inlet and switched back to wall when the run is finished.

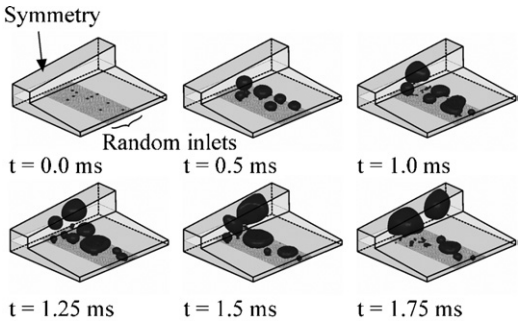

Figure 6. Simulation sequence with distributed bubble sources and bubble removal due to capillary forces.

changes the inlets back to a wall boundary. Then, ten new surfaces are selected and changed into an inlet boundary. The initial condition for the new simulation run is set to be the last result of the previous simulation sequence. This procedure is repeated several times as sketched in figure 5 with a lower number of addressable surfaces.

The results of the simulation exhibit the anticipated bubble behaviour as displayed in figure 6 where the gas is indicated in dark grey. The bubbles grow randomly in the channel and once they touch the upper wall they start to move towards the central part of the channel wiping off other bubbles on their way. Once the bubble in the central part has grown to a sufficient size, it starts to move towards the outlet of the simulation model. Thus, the simulation proves that the degassing mechanism works independently of the position where the gas is created.

4. Sample fabrication

In the preparation of the experimental part, a negative of the flowfield design with the dimensions given in figure 3(*a*) has been milled into a brass plate to form a hot embossing tool. The embossing tool is placed into a frame to prevent polymer spilling out sideways during the embossing process. Two different polymers have been chosen as substrates for the test samples: PMMA and a conductive graphite-filled polymer (SGL PPG86). The two polymers have been chosen to serve for two kinds of experiments: the transparent PMMA for experiments where the bubble development and movement is observed by a camera and the opaque, conductive graphite-filled polymer to assemble a fully functional μDMFC. After the hot embossing process, the mounting holes and the fluidic interconnections were drilled in a second step to complete the

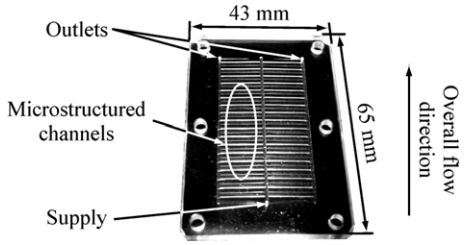

Figure 7. Photograph of one of the transparent test samples illustrating the fuel supply and the outlet channels at the edges of the microstructured array of channels.

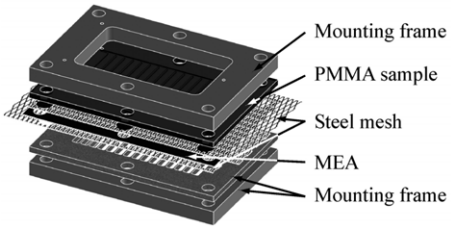

Figure 8. Assembly of the test cell for visual studies of the bubble behaviour inside the flowfield.

sample as shown in figure 7. The samples are supplied with fuel through a channel placed in the middle. CO_2 is removed through the outlet channels on the outer sides of the flowfield.

5. Experimental verification

The new flowfield layout has been tested in two different experiments. Visual studies of the bubble behaviour inside the flowfield have been performed with the transparent samples. In a second set of experiments, the graphite-filled polymer samples have been used to build a functional μDMFC.

5.1. Transparent test cell

For studying the bubble behaviour the configuration shown in figure 8 has been assembled. The setup consists of a lower mounting frame, two sheets of metal mesh interspersed with the MEA, the PMMA sample and finally an upper mounting frame. In this frame, a notch has been milled to allow direct view on the PMMA sample. To avoid methanol leakage, the stack was sealed with silicone and then tightly screwed together.

For the experiment, the metal meshes were electrically connected and the system was primed with a 2 M methanol solution that has been dyed with red ink to achieve higher contrast. By applying a current of 500 mA at a voltage of about 0.2 V between the metal meshes the creation of gas bubbles has been forced. A fuel cartridge was connected to the supply channel during the experiments to allow passive refuelling of the flowfield. The CO_2 bubbles could be released through the outlet channel located at the left margin of the photos in figure 9 that show a detail of the flowfield. During the experiment, a video camera has been used to observe the bubble behaviour. In contrast to the simulation, the bubbles first had to pass the metal mesh before they moved towards the

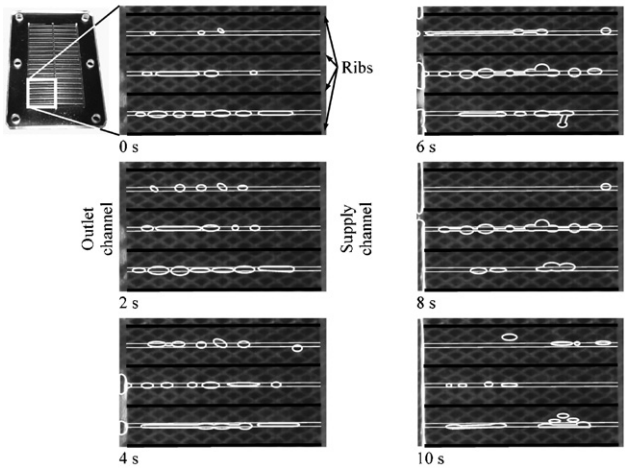

Figure 9. Picture sequence of the developing gas bubbles and their movement inside one test sample with a 2 M methanol solution. For better visualization, the spaces between each particular microchannel (ribs) are marked as black bars, while the edges of the central part of the channel and the bubbles are marked in white.

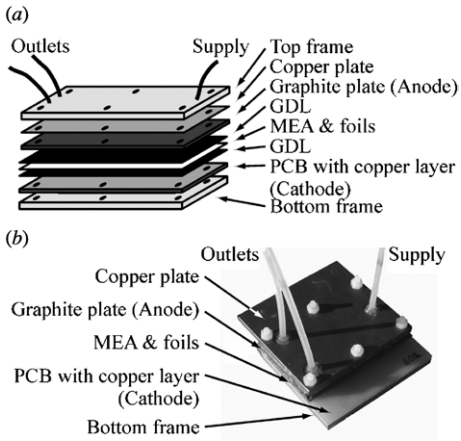

Figure 10. (*a*) Draft of the fuel cell assembly (not to scale). (*b*) Photograph of the assembled fuel cell.

central part of the microstructured channel. Since the mesh used is rather coarse, some bubbles are trapped inside the mesh until they get wiped off by another bubble or have grown to a sufficient size to detach. As predicted by the simulation the bubbles first move towards the central channel part and once there grow further until they start to move again. This time their movement is directed towards the outlet channel as anticipated.

5.2. Fuel cell assembly

For the second set of experiments with the new flowfield layout a planar fuel cell has been assembled as depicted in figure 10. The assembly differs in comparison to the cell used for the bubble behaviour experiments although the same flowfield design has been used. In this assembly, the cathode was made of ordinary printed circuit board (PCB). The PCB is a laminate of glass fibre and epoxide sandwiched between two copper layers of 35 μm thickness. In the cathode material

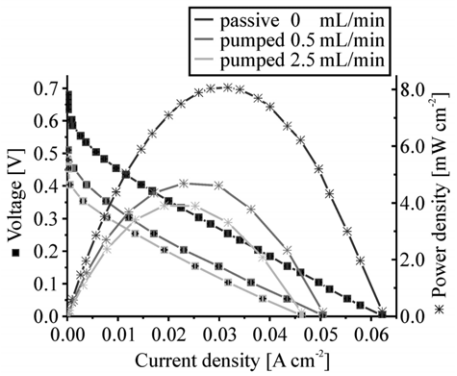

Figure 11. Short-time measurements with a 4 M methanol solution at two pumped flow rates and a passive system setup.

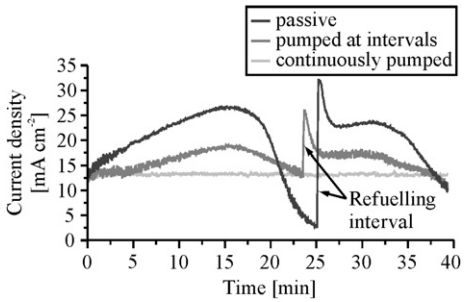

Figure 12. Long-time measurements with a 4 M methanol solution at 0.25 V. Continuously pumped (0.225 ml min^{-1}), pumping at intervals (∼23 min pause, 15 s pumping) and passive with refuelling by hydrostatic pressure after ∼25 min.

parallel rectangular openings of 3 mm × 21 mm with a spacing of 1 mm have been milled to form the cathode flowfield. Thus, the electrochemical active area of the fuel cell is 21 mm × 43 mm. The copper layer of the PCB was used as current collector and electrical contact to the outside of the fuel cell. A hot embossed and drilled graphite plate of SGL PPG86 with the flowfield structure described above has been used as the fuel cell's anode. For the electrical contact, a copper plate has been placed on the top of the graphite plate. Nafion 117 was used as the MEA with a PtRu/Pt catalyst loading of 3.5 mg cm^{-2} and an ionomer thickness of 180 μm. To avoid short circuits between the electrodes, the MEA was sandwiched between two 100 μm thick polymer foils. Instead of the metal mesh used for the transparent cell Toray carbon paper with a thickness of 350 μm was applied as the diffusion layer between the plates and the MEA. The whole assembly was pressed together by six M3 screws with a torque of 0.5 Nm each. To ensure a sufficient contact pressure between the plates, an adhesive was applied onto the edges and pressed together while curing. Furthermore, the adhesive was used to prevent leakage.

5.3. Short-time testing

Since the considered flowfield layout was designed for totally passive as well as for active, pump-assisted operation, it allows a direct comparison of the experimental results in active and passive modes. Experiments with three different flow rates have been accomplished by using a 4 M methanol solution. The flow rate of 0 ml min^{-1} is referred to as passive, since the fuel cell is only primed and run without externally forced convective flow. The flow of 0.5 ml min^{-1} respectively 2.5 ml min^{-1} was forced by an external pump. The results of this experiment as depicted in figure 11 show that the efficiency of the fuel cell increases with decreasing flow rate.

One reason for the increasing power density is the reduced methanol concentration at lower flow rates. This yields a lower methanol crossover through the membrane from the anode to the cathode side and thus a better system performance. If the pump is switched off completely an additional effect appears. The crossover is also reduced due to the lower hydraulic pressure that scales with the pump rate. This leads to an increase of the fuel cell's efficiency. Furthermore, there are two effects that depend on the temperature inside the fuel cell and the number of gas bubbles in the flowfield. Without any convective flow the temperature inside the fuel cell increases in contrast to a continuously flushed fuel cell where the flow also permanently cools the cell. The increased temperature leads to better kinetics in the cell. The second effect is connected to the phase change of methanol. As the fuel is not flushed through the flowfield together with the gas bubbles more methanol enters the vapour phase. It is well known that this leads to better kinetics on the anode and a lower crossover through the membrane [7]. Due to these reasons, it is advantageous to operate the fuel cell only with a low flow rate or even no forced flow at all.

However, operating a fuel cell without any flow would yield a power breakdown if the whole electrochemical active surface had been blocked by CO_2 bubbles or after all methanol had been oxidized (starving of the fuel cell). Concerning the CO_2 bubbles, a passive structure as described above aids the bubble removal and thus might ensure sufficient electrochemical active surface for the methanol reaction. To overcome the problem of methanol depletion, a possible solution is to pump fuel into the system at certain intervals to exchange the reaction volume and to increase the methanol concentration again. Regarding the efficiency of the fuel cell system the benefit is twofold. The fuel cell efficiency itself is higher compared to a continuously pumped system and there is no continuous energy demand for the pump as it is deactivated most of the time.

5.4. Long-time measurements

To validate the assumption of an increased efficiency by pumping at intervals long-time measurements with a 4 M methanol solution at 0.25 V have been performed. Again, three configurations have been chosen for the experiments: pumping continuously (0.225 ml min^{-1}), pumping at intervals and an open cartridge without any pump. In the case of the continuously pumped fuel cell operation, a stable current of about 14.5 mA cm^{-2} was reached as shown in figure 12. As expected, the results for the two other configurations did not show a stable current level during the extended operation. First, the current density increases for both configurations until the depletion of methanol leads to a reduction of the current density. In the configuration refuelled by pumping at intervals the fuel cell was operated for approximately 23 min and then new fuel was pumped into the system for 15 s. During the

time the pump was switched off the connection between the fuel cartridge and the cell was mechanically interrupted. Thus no methanol flowed into the cell during this time. In the last configuration, the connection between reservoir and fuel cell had been open during the whole operational time. Due to a small hydrostatic height (about 10 mm) between the cartridge and the fuel cell, a small methanol flow was allowed to flow into the cell passively during the whole measurement. As a result, the maximum performance was even better compared to the other configurations. But also for this setup the methanol depletes after a while. Therefore, after about 25 min the hydrostatic height of the cartridge was increased for a few seconds to flush new fuel into the flowfield by hydrostatic pressure. Since this last setup showed the highest current density, it indicates that a pump should be used that does not interrupt the connection between the fuel cartridge and the cell to enable passive methanol supply from the reservoir either by diffusion or by convection (e.g. driven by a small hydrostatic height difference).

6. Conclusions

A new flowfield design that allows for passive removal of gas bubbles in a μDMFC by using tapered channels with a T-shaped cross section has been proved. First, the feasibility of these channels was demonstrated with CFD simulations and then a prototype flowfield was manufactured by hot embossing techniques. Using a transparent PMMA substrate for the test samples the working principle of the flowfield layout and the passive CO_2 bubble removal could be demonstrated. Furthermore, a complete μDMFC has been assembled by using a conductive graphite-filled polymer material for the flowfield. During short-time measurements, the new flowfield design exhibited a higher efficiency when operated passively compared to the setup where methanol was continuously pumped into the system. Also in the case of long-time measurements the performance of the μDMFC refuelled at intervals of about 20 min showed a higher efficiency than the same setup when operated at a continuous pump rate. The results show that a passive removal of CO_2 bubbles by the new flowfield design allows for new methods of μDMFC operation. The efficiency for a complete passive system or a system with a fuel supply at intervals exceeds the efficiency of normal operated systems. The tested configuration where the refuelling was achieved by a hydrostatic pressure indicates that due to the passive CO_2 removal completely passively operated configurations become possible. However, this requires that the refuelling task can be solved without the use of a pump in the future.

Acknowledgments

This work was supported by the German Federal Ministry of Economics and Labour (BMWA) within the InnoNet-program (project: PlanarFC; no. 16IN0269).

References

[1] Dyer C K 2002 Fuel cells for portable applications *J. Power Sources* **106** 31–4
[2] Heinzel A, Hebling C, Muller M, Zedda M and Muller C 2002 Fuel cells for low power applications *J. Power Sources* **105** 250–5
[3] Gravesen P, Braneberg J and Jensen O S 1993 Microfluidics—a review *J. Micromech. Microeng.* **3** 168–82
[4] Kohnle J, Waibel G, Cernosa R, Storz M, Ernst H, Sandmaier H, Strobelt T and Zengerle R 2002 A unique solution for preventing clogging of flow channels by gas bubbles *Proc. IEEE MEMS (Las Vegas)* pp 77–80
[5] Laser D J and Santiago J G 2004 A review of micropumps *J. Micromech. Microeng.* **14** R35–R64
[6] Litterst C, Kohnle J, Ernst H, Messner S, Sandmaier H, Zengerle R and Koltay P 2004 Mobility of gas bubbles in CHIC-type flow channels *Proc. Actuator* ed H Borgmann pp 541–4 (Bremen)
[7] Shukla A K, Christensen P A, Hamnett A and Hogarth M P 1995 A vapor-feed direct-methanol fuel-cell with proton-exchange membrane electrolyte *J. Power Sources* **55** 87–91